Density-dependent terahertz emission in biased semiconductor superlattices: From Bloch oscillations to plasma oscillations

Lijun Yang,[1] Ben Rosam,[2] and Marc M. Dignam[1]
[1]*Department of Physics, Queen's University, Kingston, Ontario, Canada K7L 3N6*
[2]*Institut für Angewandte Photophysik, Technische Universität Dresden, 01062 Dresden, Germany*
(Received 15 June 2005; published 14 September 2005)

We present theoretical and experimental results for the density dependence of terahertz emission from undoped biased semiconductor superlattices excited via an ultrashort optical pulse. We show that exciton-exciton interactions lead to a density-dependent terahertz frequency. At low to moderate densities, the carriers undergo Bloch oscillations, with the oscillation frequency initially redshifting with increasing density. At higher densities, the Bloch oscillations transform into plasma oscillations and the oscillation frequency blueshifts with increasing density. We model the system using our excitonic Bloch equations, solved nonperturbatively in the optical field by employing a factorization scheme that allows for the inclusion of dynamic screening. We show that the observed density dependence on the terahertz frequency cannot be obtained using a method that is perturbative in the optical field.

DOI: 10.1103/PhysRevB.72.115313 PACS number(s): 78.47.+p, 42.65.Re, 73.21.Cd, 78.67.Pt

I. INTRODUCTION

The main difficulty in treating the ultrafast coherent response of semiconductor heterostructures lies in trying to calculate the response to infinite order in the optical field while retaining the key many-body effects.[1–15] On the one hand, the temporal duration of the photon-matter interaction is usually much shorter than either the dephasing or relaxation time. Thus, except in the low-field perturbation limit, the ultrafast dynamics should intrinsically be treated to infinite order in the optical field, especially when a system is resonantly excited, where such effects as Rabi flopping may occur. On the other hand, in contrast to atomic gases, many-body Coulomb correlations among quasiparticles can profoundly affect the nonlinear response in semiconductors.[2] Like in classical statistical physics, the key in quantum kinetics is to deal with an infinite hierarchy of correlation functions, the quantum version of the Bogoliubov-Born-Green-Kirkwood-Yvon (BBGKY) hierarchy. There are many ways to truncate the hierarchy such as a perturbation theory to a definite order in the optical field[6,16–18] and the cluster-expansion method,[3,8,19] which was originally employed in truncating the BBGKY hierarchies in classical statistics. Many important optical properties of semiconductors can be explained by employing just the lowest-order cluster expansion, as can been seen in the success of the semiconductor Bloch equations[3,20] (SBE's) in treating many phenomena. The first-order SBE's are basically a set of time-dependent Hartree-Fock (or mean-field) equations and thus include only static screening. Higher-order cluster expansions are necessary if one wants to account for such phenomena as dynamic screening and dephasing. Dynamic screening appears self-consistently only beyond a first-order cluster expansion.[8] Thus, it is necessary to go beyond the first-order expansion if carrier-carrier or carrier-phonon correlations play an important role in the dynamics being investigated.[5,9,21]

There are many successful quantum kinetic treatments beyond first-order cluster expansion such as those using either Green's function[22–24] or density-matrix formalism[8,25,26] in such systems as bulk semiconductors or single quantum wells. Unfortunately, the dynamic equations resulting from a higher-order cluster expansion can be computationally prohibitive for complex systems such as superlattices. Thus, one is generally forced to use a different truncation approach for such systems. One option is to employ a perturbative expansion in the optical field to a definite order. Although this has been successful in the treatment of many systems, as we will show it cannot be applied successfully to the system we are considering here, even at moderate densities. We therefore take a different approach.

In this work, we employ *an exciton basis*[27] to treat the dynamics of excitons in a biased semiconductor superlattice (BSSL). In other words, we employ a composite quasiparticle through a canonical transformation to replace the former single-particle electron and hole states. As we shall show, using an excitonic basis greatly simplifies the dynamics calculations. By using an excitonic basis, we can treat higher-order Coulomb correlations in a *much easier* and *more efficient* way than is possible in an electron-hole basis. The key approximation that we employ is to factorize a three-point exciton correlation function into the product of two-point and one-point correlation functions. This roughly corresponds to the factorization of a six-point electron-hole correlation function into the product of four-point and two-point electron-hole correlation functions and corresponds approximately to a second-order cluster expansion, where scattering effects have been neglected. This factorization allows us to include dynamic screening in the formalism, which is not accounted for in the usual first-order SBE's. The crucial feature of our approach is that the use of the exciton basis reduces enormously the computational effort needed, while still capturing the key features of the system dynamics that would be lost in a perturbative expansion in the optical field.

Although the excitonic approach has definite advantages, there has been considerable controversy in recent years regarding how to deal with the fact that the excitons are not

exact bosons, but rather are composite bosons.[28,29] The deviation of the excitons from pure bosonic behavior leads to so-called phase-space filling (PSF) effects.[28,29] However, the controversy regarding the excitonic basis is only relevant at relatively high densities, where PSF becomes important. At the densities considered in most of the results presented here, it is expected that the PSF effects will be small and thus there is no difficulty in using an excitonic approach. This is discussed in more detail in the last section.

Just as in the case of the SBE's, our approach treats the dynamics nonperturbatively in the optical field.[3,11,19] This is very important for the system being studied because, as we show, approaches that are perturbative in the optical field break down when the optical intensity is larger than a certain critical value. Perturbative approaches are widely used and can account for various optical phenomena, such as four-wave mixing (FWM) signals in BSSL's.[18] However, in BSSL's, higher-order effects have been seen both experimentally[10,15] and theoretically.[27,30] It is thus essential that a nonperturbative approach be employed in treating BSSL's when high laser intensities are used.

In this work, we will investigate the terahertz (THz) emission from a BSSL (Refs. 31 and 32) excited via ultrashort optical pulses. BSSL's are of fundamental importance for their role in furthering the understanding of transport in periodic systems and for their potential application as THz radiation sources.[33] In a single-particle picture, the electronic eigenstates of a BSSL form the so-called Wannier-Stark ladder (WSL) with the energies given by $E_n = E_0 + neF_o d$, where d is the superlattice period, F_o is the applied dc field, and n is the WSL index. Bloch oscillations (BO's) occur when wave packets are formed from a superposition of WSL states created via an ultrashort optical pulse. The BO frequency is given by $\omega_B \equiv eF_o d/\hbar$, which, in the single-particle picture, is only a function of the external dc field F_o for a given BSSL. This picture is complicated somewhat by the correlations between electrons and holes, which leads to the formation of excitons.[34] The electron-hole correlations within excitons lead to significant modifications of the single-particle WSL. However, the resulting excitonic states still retain many of the basic features of the single-particle WSL and form the so-called *excitonic* WSL (see Fig. 1). Excitation via an ultrashort optical pulse thus leads to *excitonic* BO's, which have been investigated by a large number of authors.[6,8–11,16–18,20,27,33,35] As will be shown both theoretically in this paper, the above picture begins to or even completely breaks down when the exciting optical pulse becomes intense enough that carrier interactions become important.

As discussed above, we will employ an exciton formalism to investigate the ultrafast dynamics in BSSL's. In this formalism, the carrier-carrier interactions are included at two levels. The electron-hole correlations for a single electron-hole pair are included by employing a basis of excitonic states. Then, the residual exciton-exciton interaction is included in the long-wavelength limit through a dipole-dipole interaction.[18] The exciton-exciton interaction in the BSSL amounts to a self-induced internal electric field that can significantly modify the nonlinear response of the system. The effect of this internal intraband field is particularly large in BSSL's due to the asymmetry introduced by the applied dc field. It is this asymmetry that leads to the very large nonlinearities we observe. The key theoretical and experimental results in this work are the following: as the pulse intensity is increased, the BO frequency begins to redshift due to the reduction of the applied dc field via the dc part of the excitonic intraband polarization. As the intensity is increased further, *dynamic* screening begins to play a significant role and we find that a competition arises between BO's and plasma oscillations (PO's). Finally, we show theoretically that at very high intensities, the BO's completely disappear and the dynamics becomes essentially pure PO's. As we shall show, none of key experimental effects in this work can be described satisfactorily via perturbation theory, but are described very well within our nonperturbative formalism. We compare our calculated results to experimental results and to results using fourth-order perturbation theory. We find good agreement between our nonperturbative theory and experiment and show that a perturbative approach fails to reproduce many experimentally observed features, even at moderate excitation densities.

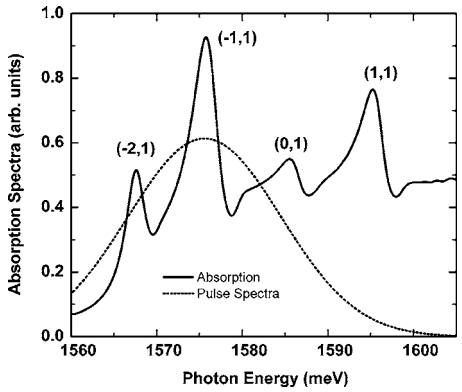

FIG. 1. The calculated linear absorption spectrum for the BSSL with a bias field of $F_o = 11.5$ kV/cm. Also shown is the power spectrum of the transform-limited Gaussian optical pulse used in all calculations and experiments. The state labelling is described in Sec. III.

The paper is organized as follows. First, in Sec. II, we present the formalism for treating intraband dynamics both perturbatively and nonperturbatively. Then, in Sec. III, we look at the induced dc field and energy conservation to show that, for high to moderate densities, only the nonperturbative theory produces physical results. In Sec. IV, we present theoretical and experimental results for the intensity dependence of the frequency of the emitted THz radiation. In Sec. V, we show theoretically that at very high intensities, plasma oscillations appear. Finally, in Sec. VI, we summarize our findings.

II. DYNAMIC EQUATIONS

In this section, we derive the equations of motion of the excitonic correlation functions used to calculate the intraband and interband response of a BSSL. We begin by presenting the excitonic Hamilton that we developed in earlier work.[18,27] We then use this Hamiltonian to derive both the

perturbative and nonperturbative equations of motion for the correlation functions.

A. System Hamiltonian

We express our system Hamiltonian in the basis of excitonic states, which are the electron-hole eigenstates of the superlattice in the presence of an applied dc field, F_o. These include the $1s$-like excitonic Wannier-Stark ladder states as well as higher in-plane excitonic states, including continuum electron-hole pair states. Treating the exciton-exciton interaction in the long-wavelength dipole approximation, the Hamiltonian is given by[18,27]

$$H = \sum_{\mu} \hbar\omega_{\mu} B_{\mu}^{\dagger} B_{\mu} + V\left(- \mathbf{E}_{\text{opt}} \cdot \mathbf{P}_{\text{inter}} + \frac{1}{2\varepsilon} \mathbf{P}_{\text{intra}} \cdot \mathbf{P}_{\text{intra}} \right), \tag{1}$$

where V is the volume of the system, ϵ is the static dielectric constant and $B_{\mu}^{\dagger}(B_{\mu})$ is the creation (annihilation) operator for a WSL exciton in the dc field, with internal quantum number μ and energy $\hbar\omega_{\mu}$. The optical field takes the form

$$\mathbf{E}_{\text{opt}}(t) = \mathcal{E}(t) e^{-i\omega_c t} + \text{c.c.}, \tag{2}$$

where ω_c is the central laser frequency and $\mathcal{E}(t)$ is the ultrafast optical pulse envelope. The polarization operator is defined as

$$\mathbf{P} \equiv \mathbf{P}_{\text{inter}} + \mathbf{P}_{\text{intra}}, \tag{3}$$

where $\mathbf{P}_{\text{inter}}$ and $\mathbf{P}_{\text{intra}}$ denote, respectively, the interband and intraband polarization. The interband polarization is defined as

$$\mathbf{P}_{\text{inter}} \equiv \frac{1}{V} \sum_{\mu} [\mathbf{M}_{\mu} B_{\mu}^{\dagger} + \mathbf{M}_{\mu}^{*} B_{\mu}], \tag{4}$$

where

$$\mathbf{M}_{\mu} = \mathbf{M}_0 \sqrt{A} \int dz \psi^{\mu *}(z,z,0) \tag{5}$$

is the interband dipole matrix element of the μth excitonic state, $|\psi^{\mu}\rangle$, where $\mathbf{M}_0$ is the bulk interband dipole matrix element and A is the transverse area. The intraband polarization is defined as

$$\mathbf{P}_{\text{intra}} \equiv \frac{1}{V} \sum_{\mu,\mu'} \mathbf{G}_{\mu,\mu'} B_{\mu}^{\dagger} B_{\mu'}, \tag{6}$$

where $\mathbf{G}_{\mu\mu'}$ is the intraband dipole matrix element between two excitonic states $|\psi^{\mu}\rangle$ and $|\psi^{\mu'}\rangle$, given by

$$\mathbf{G}_{\mu\mu'} = \langle \psi^{\mu} | - e(z_e - z_h) | \psi^{\mu'} \rangle. \tag{7}$$

The detailed derivations of these expressions for the polarization are given in our earlier work.[18] We finally note that the dependence of the excitonic states on the exciton center of mass wave vector was neglected in the above Hamiltonian. This is valid since we are only considering single-pulse excitation, where all the optically generated excitons have the same momentum, given by the tiny photon momentum.

B. Nonperturbative equations

Using the exciton Hamiltonian of Eq. (1), we first derive the dynamic equations for the exciton creation operator $B_{\mu}^{\dagger}$ from the Heisenberg equation of motion. Taking the expectation value of the equation of motion and adding a phenomenological interband dephasing time constant, $T_{\mu} = T_{2\text{inter}}$, we obtain

$$i\hbar \frac{d\langle B_{\mu}^{\dagger} \rangle}{dt} + \hbar \left(\omega_{\mu} + \frac{i}{T_{\mu}} \right) \langle B_{\mu}^{\dagger} \rangle - \mathbf{E}_{\text{opt}} \cdot \mathbf{M}_{\mu}^{*} = - \frac{1}{\varepsilon_0 \varepsilon} \frac{1}{V} \sum_{\mu',\mu'',\mu'''} \mathbf{G}_{\mu'',\mu'''} \cdot \mathbf{G}_{\mu',\mu} \langle B_{\mu''}^{\dagger} B_{\mu'''} B_{\mu'}^{\dagger} \rangle. \tag{8}$$

Solving this equation would require the solution to the equation of motion for $\langle B_{\mu''}^{\dagger} B_{\mu'''} B_{\mu'}^{\dagger} \rangle$, which in turn would require equations of motion for five operator correlation functions and so on. This, therefore leads to an infinite hierarchy of equations. There are two common ways to truncate such hierarchies: (i) adopt a factorization scheme or (ii) apply perturbation theory in the optical field. In this section, we employ a factorization, while in the next we use perturbation theory.

The factorization scheme that we use for the triple-operator term is

$$\langle B_{\mu''}^{\dagger} B_{\mu'''} B_{\mu'}^{\dagger} \rangle = \langle B_{\mu''}^{\dagger} B_{\mu'''} \rangle \langle B_{\mu'}^{\dagger} \rangle. \tag{9}$$

This factorization is similar to the random-phase or Hartree-Fock approximation used in deriving the semiconductor Bloch equations.[3] However, because we are using the excitonic basis, our approximation is preferable for the current system because it fully retains the electron-hole correlations within an exciton.[18,27] Using this in Eq. (8), we obtain

$$i\hbar \frac{d\langle B_{\mu}^{\dagger} \rangle}{dt} + \hbar \left(\omega_{\mu} + \frac{i}{T_{\mu}} \right) \langle B_{\mu}^{\dagger} \rangle - \mathbf{E}_{\text{opt}} \cdot \mathbf{M}_{\mu}^{*} = \mathbf{E}_{\text{intra}} \sum_{\mu'} \mathbf{G}_{\mu',\mu} \langle B_{\mu'}^{\dagger} \rangle, \tag{10}$$

where

$$\mathbf{E}_{\text{intra}} \equiv - \frac{1}{\varepsilon_0 \varepsilon} \langle \mathbf{P}_{\text{intra}} \rangle \tag{11}$$

is the induced intraband electric field in the structure. The term on the right-hand side (RHS) of Eq. (10) originates from the exciton-exciton interaction term $(1/2\varepsilon)\mathbf{P}_{\text{intra}} \cdot \mathbf{P}_{\text{intra}}$ in the Hamiltonian [Eq. (1)]. Therefore, within our formalism, the exciton-exciton interaction in the BSSL system amounts to a self-induced electric field $\mathbf{E}_{\text{intra}}$ within the superlattice.

Using the factorization scheme

$$\langle B_{\mu''}^{\dagger} B_{\mu'''} B_{\mu'}^{\dagger} B_{\nu} \rangle = \langle B_{\mu''}^{\dagger} B_{\mu'''} \rangle \langle B_{\mu'}^{\dagger} B_{\nu} \rangle, \tag{12}$$

we obtain from Eq. (1) the intraband equation of motion:

$$i\hbar\frac{d\langle B_\mu^\dagger B_\nu\rangle}{dt} = -\hbar\left(\omega_\mu - \omega_\nu + \frac{i}{T_{\mu\nu}}\right)\langle B_\mu^\dagger B_\nu\rangle + \mathbf{E}_{\text{opt}}\cdot[\mathbf{M}_\mu^*\langle B_\nu\rangle - \mathbf{M}_\nu\langle B_\mu^\dagger\rangle] + \mathbf{E}_{\text{intra}}\sum_{\mu'}(\mathbf{G}_{\mu',\mu}\langle B_{\mu'}^\dagger B_\nu\rangle - \mathbf{G}_{\mu',\nu}^*\langle B_\mu^\dagger B_{\mu'}\rangle), \tag{13}$$

where $T_{\mu\nu}$ is the intraband dephasing constant, T_{2intra} when $\mu \neq \nu$, and the exciton population lifetime T_{1ex} when $\mu = \nu$. After solving the set of coupled Eqs. (10) and (13), we obtain the intraband polarization by taking the expectation value of Eq. (6). The THz signals are then obtained by taking the second derivative of this intraband polarization.

The factorization in Eq. (12) is of key importance in our formalism. Although this results in the loss of biexciton correlations, the factorization makes it possible for us to treat the dynamics to infinite order in the optical field—i.e., nonperturbatively. As we will show, this nonperturbative approach is necessary to account for the experimental results in the case of high optical excitation. In Eq. (13), the local self-generated intraband electric fields $\mathbf{E}_{\text{intra}}$ defined in Eqs. (6) and (11) depend only on the correlation functions $\langle B_\mu^\dagger B_\nu\rangle$. Therefore, by using the factorization in Eq. (12), the local fields $\mathbf{E}_{\text{intra}}$ are in fact treated self-consistently. In other words, any change of the intraband local fields is fed back to the dynamic equations self-consistently. This allows the instantaneous net electric field to directly affect the exciton dynamics.

Generally, most methods in treating quantum kinetics are either perturbative in the optical field, but keep as many of the Coulomb correlations as possible, or are nonperturbative in the optical field, but keep certain types of Coulomb correlations up to definite orders. However, it is impossible to be nonperturbative in the both optical field and all types of Coulomb correlations. When the optical field is larger than a certain critical value, then it is preferable to treat the system to infinite order in the optical field *at the cost of losing higher order Coulomb correlations*. We refer to our approach as a *nonperturbative approach*, in that it is *nonperturbative in the optical field*. Our approach is similar to the recent work of Axt and Mukamel on molecular systems,[11] except that we neglect phase-space filling and explicitly employ the intraband polarization, which greatly reduces the computational effort. Because we use an excitonic basis, our approach cannot be compared directly to recent cluster-expansion approaches.[8] However, roughly speaking, our approach corresponds to a second-order cluster expansion, where dynamic screening is included, but carrier-carrier scattering is neglected. In deriving the above equations of motion, we have assumed that the excitons are bosons and have thus neglected PSF effects. These effects can be taken into account using our formalism by using nonbosonic commutation relations.[18] However, it can be estimated that these phase-space filling effects will not play a significant role until densities are well above 10^{10} cm^{-2} per period. Although it is preferrable to include PSF effects as in other works employing an exciton basis,[11,36] to treat the intraband dynamics self-consistently while still including the PSF effects would make the calculations completely intractable in the BSSLs investigated.

C. Perturbation theory equations

To demonstrate the necessity of employing a nonperturbative approach at moderate to high densities, we wish to compare the results from our nonperturbative theory with perturbation theory results. Thus, we now derive dynamic equations using perturbation theory to second[16,17] and fourth order in the optical field.

We expand the exciton creation operator as

$$B_\mu^\dagger = B_\mu^{\dagger(1)} + B_\mu^{\dagger(2)} + B_\mu^{\dagger(3)} + \cdots, \tag{14}$$

where the superscripts describe the order in the optical field. Using the Heisenberg equations of motion and employing factorizations similar to that of Eq. (9), we obtain the following equations of motion for describing the intraband dynamics up to fourth order in the optical field:

$$i\hbar\frac{d\langle B_\mu^\dagger\rangle^{(1)}}{dt} = -\left(\hbar\omega_\mu + \frac{i\hbar}{T_\mu}\right)\langle B_\mu^\dagger\rangle^{(1)} + \mathbf{E}_{\text{opt}}\cdot\mathbf{M}_\mu^*, \tag{15}$$

$$i\hbar\frac{d\langle B_\mu^\dagger B_\nu\rangle^{(2)}}{dt} = -\left(\hbar\omega_\mu - \hbar\omega_\nu + \frac{i\hbar}{T_{\mu\nu}}\right)\langle B_\mu^\dagger B_\nu\rangle^{(2)} + \mathbf{E}_{\text{opt}}\cdot[\mathbf{M}_\mu^*\langle B_\nu\rangle^{(1)} - \mathbf{M}_\nu\langle B_\mu^\dagger\rangle^{(1)}], \tag{16}$$

$$i\hbar\frac{d\langle B_\mu^\dagger\rangle^{(3)}}{dt} = -\left(\hbar\omega_\mu + \frac{i\hbar}{T_\mu}\right)\langle B_\mu^\dagger\rangle^{(3)} + \mathbf{E}_{\text{intra}}^{(2)}\cdot\sum_{\mu'}\mathbf{G}_{\mu',\mu}\langle B_{\mu'}^\dagger\rangle^{(1)}, \tag{17}$$

$$i\hbar\frac{d\langle B_\mu^\dagger B_\nu\rangle^{(4)}}{dt} = -\left(\hbar\omega_\mu - \hbar\omega_\nu + \frac{i\hbar}{T_{\mu\nu}}\right)\langle B_\mu^\dagger B_\nu\rangle^{(4)} + \mathbf{E}_{\text{opt}}\cdot[\mathbf{M}_\mu^*\langle B_\nu\rangle^{(3)} - \mathbf{M}_\nu\langle B_\mu^\dagger\rangle^{(3)}] + \mathbf{E}_{\text{intra}}^{(2)}\cdot\sum_{\mu'}[\mathbf{G}_{\mu',\mu}\langle B_{\mu'}^\dagger B_\nu\rangle^{(2)} - \mathbf{G}_{\mu',\nu}^*\langle B_\mu^\dagger B_{\mu'}\rangle^{(2)}]. \tag{18}$$

The intraband polarizations up to second and fourth order in the optical field are given, respectively, by

$$\langle\mathbf{P}_{\text{intra}}^{(2)}\rangle \equiv \frac{1}{V}\sum_{\mu,\mu'}\mathbf{G}_{\mu,\mu'}\langle B_\mu^\dagger B_{\mu'}\rangle^{(2)}, \tag{19}$$

$$\langle\mathbf{P}_{\text{intra}}^{(4)}\rangle \equiv \frac{1}{V}\sum_{\mu,\mu'}\mathbf{G}_{\mu,\mu'}[\langle B_\mu^\dagger B_{\mu'}\rangle^{(2)} + \langle B_\mu^\dagger B_{\mu'}\rangle^{(4)}]. \tag{20}$$

The term $\mathbf{E}_{\text{intra}}^{(2)}$ in Eqs. (17) and (18) is defined as

$$\mathbf{E}_{\text{intra}}^{(2)} = -\frac{1}{\varepsilon_0\varepsilon}\langle\mathbf{P}_{\text{intra}}^{(2)}\rangle. \tag{21}$$

The corresponding THz signals up to second- and fourth-order optical responses are obtained by taking a second de-

rivative with respect to time. We note that in addition to factorizations of the form given in Eq. (9), we have also employed four operator factorizations of the form

$$\langle B^{\dagger(1)}_{\mu''} B^{(1)}_{\mu'''} B^{\dagger(1)}_{\mu'} B^{(1)}_{\nu} \rangle = \langle B^{\dagger}_{\mu''} B_{\mu'''} \rangle^{(2)} \langle B^{\dagger}_{\mu'} B_{\nu} \rangle^{(2)}. \quad (22)$$

Although strictly speaking we do not need to employ factorization in the fourth-order equations, we use the factorizations because they speed up the calculations enormously. We have shown in previous work[18] that they have only a very small effect on the calculated polarizations.

III. COMPARISON OF PERTURBATIVE AND NONPERTURBATIVE RESULTS

In this and all following sections, the structure we investigate both theoretically and experimentally is an undoped $GaAs/Ga_{0.3}Al_{0.7}As$ superlattice with well width of 6.7 nm and barrier width of 1.7 nm. The physical parameters used in calculations are given in Ref. 34. The applied dc field is taken as 11.5 kV/cm in all calculations and is estimated as 12 ± 0.5 kV/cm in the experimental setup. This gives a WSL energy spacing of approximately 10 meV and a corresponding BO frequency of 2.4 THz.

We use Eqs. (10), (13), and (15)–(18), to calculate the emitted THz electric field when the BSSL is excited by an ultrashort optical pulse. In this section we compare the ultrafast dynamics of the BSSL calculated to second order, fourth order, and nonperturbatively in the optical field. We then discuss the conditions under which finite-order perturbation theory breaks down.

In the dynamics calculations, $1s$ and higher s-like in-plane excitonic states (HIES's) in BSSL's are all included. These states are calculated using the two-well excitonic states described in Ref. 16. To obtain convergence, we need to consider at least 10^3 internal states. Thus, at least 10^6 dynamics equations have to be solved simultaneously. The inclusion of HIES's is particularly important in modeling the dynamics in BSSL's. Even in the low exciton density limit, the HIES's can qualitatively modify the intraband dynamics of BSSL's, as shown in Ref. 16. We only include the heavy-hole excitonic states in our calculations as these dominate the response for the conditions considered here. Although the excitonic states are very complicated,[16] for the convenience of discussion they can be approximately labeled by the index pair $\mu=(n,m)$, where n indicates the approximate WSL index of the exciton and m gives the dominant quantum number for in-plane motion. In this scheme, the intraband dipole of the (n,m) state in the z direction is approximately $-ned$, where $n=\ldots,-2,-1,0,1,2,\ldots$, as is the case for single-particle WSL states. The states with $m=1$ are $1s$-like excitonic states, while the states with $m>1$ correspond to HIES's with s-symmetry, up to continuum states.

We emphasize here that employing an exciton basis is very critical in modeling the BSSL's. This allows us to include the electron-hole correlations within an exciton exactly. Furthermore, we capture the dynamic screening portion of the second-order Coulomb correlations, which is essential in accounting for the experimental phenomena being investigated. Employing such a basis also increases the calculation efficiency enormously relative to an electron-hole basis and thus makes the problem tractable. In Ref. 16, we presented an efficient way for calculating the exciton basis including both bound and unbound excitons up to continuum states. It involves two matrix diagonalization processes: calculating a two-well exciton basis first and then using this two-well basis to calculate the final BSSL excitonic basis. Such a method for calculating the full excitonic basis is efficient in the sense that once the two-well basis is obtained for a certain structure, we can obtain the final exciton basis for a given applied dc field by a further diagonalization that is relatively fast. We do not need to recalculate the two-well basis each time the dc field is changed. Furthermore, once the exciton basis is obtained, we can calculate the intraband dynamics quite rapidly (approximately 2 h on a 3-GHz Xenon processor for a single curve). However, if we were to employ an electron and hole basis to directly calculate the intraband dynamics of BSSL's, the calculation time would be much longer, as the first-order correlations between electrons and holes essentially have to be recalculated again for each excitation condition in the dynamics calculations. In summary, the key feature of our method employing an exciton basis is that we automatically include the electron-hole correlations within an exciton, thereby allowing us to efficiently calculate intraband dynamics with only first-order two-operator excitonic correlation functions, rather than the four-operator correlation functions required in an electron-hole basis.

The optical pulse used throughout this work to excite the system both in theory and experiments is a transform-limited 86-fs Gaussian pulse with a spectral full width at half maximum (FWHM) of 21 meV and a central frequency centered on $\omega_c=\omega_{(-1,1)}$, which corresponds to the $n=-1$ $1s$ excitonic WSL state. We present in Fig. 1 the calculated absorption spectrum and the pulse power spectrum for the dc field and optical pulse used in this work. The $1s$-like heavy-hole WSL excitonic states are labeled by the indices $(n,1)$.

The optical pulse has been chosen so as to excite a superposition of $1s$-like WSL states as well as a portion of the continuum. We expect such a pulse to excite Bloch-oscillating excitonic wave packets. Thus, the induced intraband field E_{intra} will contain an ac portion oscillating at THz frequencies corresponding to Bloch oscillations. However, it will also contain a dc portion that will persist as long as the excitonic population is present. This dc component arises because a BSSL is an asymmetric system, with the applied dc field introducing a strong asymmetry into the envelope functions of the excitonic eigenstates. Thus, in general these eigenstates have relatively large permanent intraband dipole moments [$\simeq -end$ for state (n,m)].

When an optical pulse creates an excitonic population, the excitonic permanent dipoles result in a generation of an induced intraband dc field E_{dc}. In this section alone, we set the excitonic lifetime T_{1ex} to be infinite to facilitate the comparison of results from the different calculation methods. Thus after the optical pulse has passed, the dc component of the intraband field remains constant. We now want to consider the dependence of this induced dc field on excitonic density.

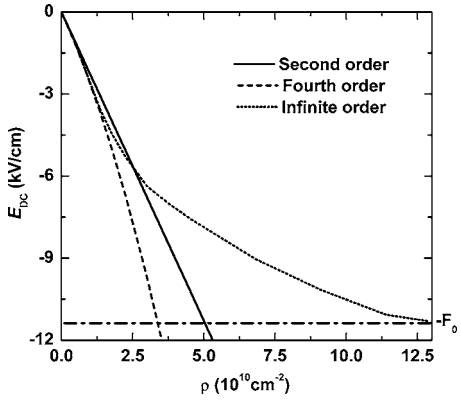

FIG. 2. Calculated induced internal dc field E_{dc} as a function of the exciton areal density ρ.

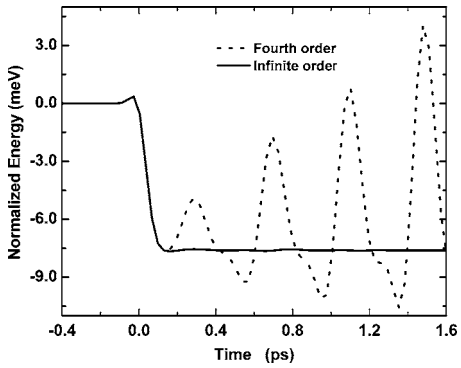

FIG. 3. Total energy per exciton as a function of time for the fourth-order, and nonperturbative (infinite order) calculations.

As we have discussed in earlier papers,[16] when the central laser frequency is below the transition frequency $\omega_{(0,1)}$ of the $n=0$ $1s$ excitonic WSL state, the photogenerated excitons largely have dipoles that point in the $+z$ direction and the net dc component E_{dc} of the induced field opposes the original external dc field F_o. This induced field depends on the exciton density excited by the ultrafast optical pulse. As the pulse is absorbed, the total dc field, F_o+E_{dc}, will get smaller and smaller (because E_{dc} opposes F_o). Thus, excitons that are created at later times will be created in a smaller field than those at earlier times. They will therefore have, on average, a smaller permanent dipole. In fact, in the limit that the total dc field is zero, they will have no net dipole in z direction. Furthermore, if the net field were to reverse, they would have a net dipole that would add to the external field. Thus it is clear that in the limit of high density, the induced dc field should be equal to the negative of the applied field—i.e., $E_{dc}\rightarrow -F_o$. Thus, regardless of the optical intensity (and hence generated excitonic density), the net internal dc field can approach zero but should never be negative. Therefore any accurate method for treating ultrafast dynamics in a BSSL or any other asymmetric structure (such as a biased quantum well or biased coupled-double quantum wells) must ensure this limit.

In Fig. 2, we plot the induced dc field E_{dc} as a function of exciton density for second-order, fourth-order, and nonperturbative (infinite order) calculations. The densities ρ given in all that follows are the peak exciton areal densities per period. To second order (and to a good approximation to infinite order as well), the density is proportional to the optical pulse energy (or peak intensity). In these calculations, we take the interband and intraband dephasing times to be $T_{2\text{inter}}=0.33$ ps and $T_{2\text{intra}}=0.52$ ps, respectively. We see that in the second-order simulations, E_{dc} decreases linearly with respect to density. This occurs because there are no exciton-exciton interactions to second order. Therefore, the total induced dc field E_{dc} is just the sum of dc fields arising from all of the induced excitons, which are all created in the same net dc field F_o. Thus, the induced field to second order is exactly proportional to the density.

The E_{dc} calculated via the fourth-order simulations decreases even faster with density than in the second-order ones and therefore does not guarantee that the net dc field, F_o+E_{dc}, is greater than zero. In contrast, the E_{dc} calculated in the nonperturbative simulations indeed approaches the saturation limit of $-F_o$, as shown in the dash-dotted line in Fig. 2. The nonperturbative result produces the physically correct result because the self-induced field $\mathbf{E}_{\text{intra}}$ provides negative feedback in the dynamic equations [Eqs. (10) and (13)]. In contrast, there is no direct feedback in the fourth-order equations, with the second-order intraband response [Eq. (16)], for example, being completely independent of the induced intraband field. We note that the nonperturbative calculations are not fully converged for carrier density between 1.25×10^{10} cm^{-2} and 10.0×10^{10} cm^{-2} for the basis size used. The reasons for this are discussed in Sec. V. However, results are converged at high densities where the correct limit is found. Furthermore, we find that regardless of the basis size employed, the calculated net internal dc field never goes below zero.

As further evidence of the necessity of employing a nonperturbative method when we reach moderate to high exciton densities, we now consider conservation of energy using the two methods. If the exciton population decay time and all of the dephasing time constants are set to infinity, then it is clear from the Hamiltonian that the total energy of the system should be conserved once the exciting optical pulse has passed. This energy includes both the single exciton energies and the exciton-exciton interaction energy.

We plot in Fig. 3 the total energy of the system normalized to the final exciton density as a function of time for fourth-order and nonperturbative calculations for an exciton density of 1.0×10^{10} cm^{-2}. The energy is taken relative to (0, 1) excitonic state (see Fig. 1). Thus, after the optical pulse has passed, this quantity is the total energy per exciton relative to the $n=0$ $1s$ heavy-hole exciton. In these calculations, we have set all dephasing and lifetimes to infinity. In the nonperturbative results, we find that the energy is constant once the pulse has passed, a result that can easily be proven analytically from the nonperturbative equations of motion. In this case, the exciton populations are driven up and down the WSL by the induced intraband field in such a way that the resulting change in the noninteracting excitonic energy [first term in Eq. (1)] exactly balances out the change in the interaction energy. In the fourth-order results—the lowest order

which includes the exciton-exciton interactions in any way—the energy is clearly not conserved, even after the optical pulse has passed, with fluctuations in the energy being as large as 13 meV, which is larger than the WSL spacing. In this case there is no such balance and the oscillations in the interaction energy (essentially due to the BO's) become much larger than the oscillations in the bare excitonic energies. The fourth-order method will only yield even approximate conservation of energy when the interaction energy is much less than the total bare exciton energy. In fact, even for an exciton density as low as $\rho=0.2\times10^{10}$ cm^{-2}, the oscillations in the total energy per exciton are still roughly 1.1 meV ($\sim$10% of the WSL spacing). Thus, it would appear that the fourth-order results are only valid when the exciton density is below $\rho=0.2\times10^{10}$ cm^{-2}. For such densities, the induced dc field is less than 5% of the applied dc field.

From the above discussion, it is evident that a nonperturbative formalism is necessary in treating intraband dynamics in BSSL's for moderate to high densities. Perturbation methods cannot guarantee the saturation limit of the self-induced dc electric field and cannot yield energy conservation. The perturbation methods are only valid when the excitation density is very low and thus the internally induced dc field is negligible. For the system considered here this will be the case if $\rho<0.2\times10^{10}$ cm^{-2}. As we show in the following sections, the higher-density phenomena of the BO frequency redshift and coherent PO's can only be accounted for through nonperturbative calculations.

IV. BLOCH OSCILLATION REDSHIFT

In this section we present experimental and theoretical results demonstrating the redshift of the BO frequency with density. The experiments were performed on the BSSL described in the previous section.[35] The THz radiation emitted into free space was detected by electro-optic sampling[37] using a gating pulse with a duration of 70 fs. A $\langle110\rangle$ cut ZnTe crystal with a thickness of 250 μm was employed as electro-optic detector, which has a sharp frequency cutoff at around 4 THz.[38] The sample was mounted (tilted by 50°) in a cryostat and held at a temperature of 10 K.[35] The THz radiation emitted in the direction of the transmitted pump beam was imaged by two pairs of gold-coated off-axis parabolic mirrors. At the position of a THz focus (in between the second and third mirrors) a chopper was placed to modulate the THz radiation. The signal was detected in a shot-noise-limited balanced detection scheme.[39] The pump beam was the 21-meV-wide transform-limited Gaussian pulse discussed in the previous section. In addition to the intense pump beam, a weak, spectrally broad pulsed monitor beam was also coupled in, which spatially overlapped with the pump spot on the sample and arrived at the sample before the pump beam. The transmission spectrum of the monitor beam was measured to monitor and control the internal dc field of the sample present before the pump beam hit the sample. In this way we are certain that the applied dc field present before the arrival of the pump beam is the same for all pump intensities. The excitation density was calculated from the measured laser spot size and the dc photocurrent extracted from the sample.

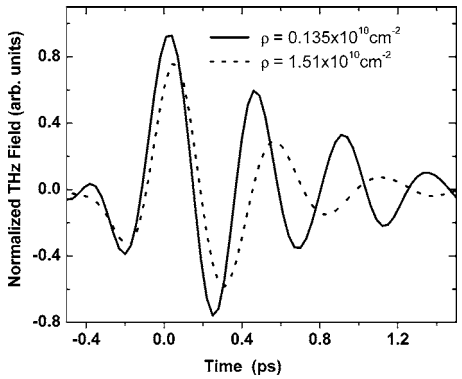

FIG. 4. The experimentally obtained emitted THz signal per exciton as a function of time for two different exciton densities.

The normalized experimental THz emission signals for two different exciton densities are shown in Fig. 4. In this figure and all subsequent figures where we refer to normalized results, the emitted THz electric field is divided by the peak excitonic density; i.e., the normalized signal is the THz field per exciton. For both densities, the BO's clearly persist for at least four oscillations. However, the THz signal emitted in the experiment with the higher exciton density has a significantly lower frequency. In other words, the frequency is redshifted as the excitation density is increased. This redshift can be seen more clearly in Fig. 5, where we plot the amplitude of the Fourier transform of the (un-normalized) experimental THz field for different exciton densities. As the exciton density is increased, the spectral peak first experiences a redshift, with the BO frequency decreasing almost linearly with the density. As the density is increased further, the rate at which the BO peak frequency shifts slows, until it saturates at a frequency of about 1.89 THz when the density reaches about 1.5×10^{10} cm^{-2}. Finally, at higher density still (2.02×10^{10} cm^{-2}), a slight blueshift in the BO frequency appears.

We now present our nonperturbative and fourth-order theoretical results for the above experiments and show that the observed experimental phenomena are only well accounted for via the nonperturbative model. In these and all subsequent calculations, the interband and intraband dephasing

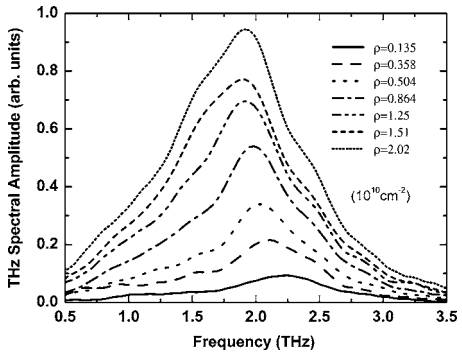

FIG. 5. The amplitude of the Fourier transform of the (un-normalized) experimental THz electric fields for different exciton areal densities.

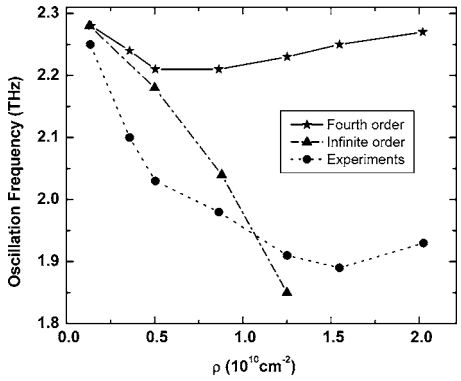

FIG. 6. The peak THz frequency as a function of the exciton density for the experimental results, and the fourth-order and nonperturbative (infinite order) calculations.

times are taken to be $T_{2\text{inter}}=0.33$ ps and $T_{2\text{intra}}=0.52$ ps, respectively, to agree with those estimated from the experimental results. The exciton population life time is taken to be $T_{1ex}=1$ ps. As defined in Eq. (13), the exciton lifetime here refers to the time that an exciton remains in a *particular* excitonic eigenstate; it is not the recombination time for an exciton, which is much longer. Because there is no ground state for an exciton in a BSSL, these times can be considerably shorter than the recombination lifetime. There is no simple way of determining this lifetime unless we include the microscopic treatment for exciton-exciton and exciton-phonon scattering. Fortunately, we find that the precise choice of this lifetime does not qualitatively affect the results as long as it is larger than the intraband dephasing time. We have found that even we choose the lifetime to be infinite, the final results are not qualitatively changed. The particular choice of $T_{1ex}=1$ ps was made because it is consistent with experimental results in the literature and it results in good computational convergence.

Figure 6 shows the BO peak frequency as a function of density for the experimental results and fourth-order and nonperturbative calculations. The second-order result is not shown because its frequency is density independent. The fourth-order and nonperturbative calculations give the same results as that of second-order calculations when the excitation density is very low. However, as the excitation density is increased, the results of second- and fourth-order calculations differ greatly from the nonperturbative results. As shown in Fig. 6, although there is a redshift in the fourth-order calculations, the size of the shift is very small compared to the experimentally obtained shift. The nonperturbative calculations, however, are in quite good agreement with experiment over the range of densities for which we have performed calculations. The differences between the peak shifts found in the experimental and theoretical results likely arise largely from uncertainties in a number of experimental parameters such as the carrier density, the dc electric field, and the exciton lifetimes. Given these uncertainties, we feel that the agreement is quite satisfactory.

There are two main contributing factors to the redshift in the BO frequency. The first is the ultrafast creation of a dc field arising from the photoexcitation of excitons with permanent intraband dipole moments, as discussed in the previous section. This induced dc field changes the energy separation of the excitonic WSL states and hence changes the BO frequency observed in the emitted THz radiation. Because the induced dc field opposes the applied field, the *net* field decreases with increasing density and the BO frequency redshifts. This effect alone results in the almost linear dependence of the BO frequency on density that is seen in experiment and nonperturbative results at low density. A more recent experiment[40] reported a similar effect in strongly biased single quantum wells. However, to our knowledge, our work presents the first measurement of the effect of an density-dependent ultrafast dc field on the *coherent evolution* of a photoexcited wave packet and is the first quantitative theory presented for this evolution.

The second potential mechanism affecting the BO frequency is the *dynamic* screening of the applied dc field. Previous experimental work has investigated the THz frequency chirping due to the dynamic screening.[41] It has also been shown both theoretically[42,43] and experimentally[44] that the response time for ultrafast dynamic screening is given approximately by the inverse of the plasma frequency. By extrapolating the results presented in the next section to low densities, we find that this response time is roughly 3.6 ps for densities of $\rho=2\times10^9$ cm^{-2} and decreases as the square root of the density to roughly 1.2 ps for the highest density of $\rho=1.25\times10^{10}$ cm^{-2}. Given that the Bloch oscillations only persist for times on the order of 1.2 ps, it would appear that dynamic screening effects should only start to be evident at densities on the order of $\rho\geqslant5\times10^9$ cm^{-2}. This is evident in the slightly nonlinear response of the density dependence of the BO frequency in the nonperturbative results and in experiment. We are not certain why the calculated results seem to be redshifting superlinearly in this density range, while the experimental results are redshifting sublinearly. However, it is likely that better agreement would only be achieved if the phenomenological dephasing and relaxation were replaced by microscopic scattering mechanisms. However, as we discuss in the following section, our theoretical results at higher densities indicate that the BO frequency will eventually saturate and will finally blueshift as the density is increased. Thus, even these effects are qualitatively accounted for in our theory.

We have not presented the calculated the THz emission for densities larger than 1.25×10^{10} cm^{-2} because we find that the nonperturbative results do not converge for densities in the range 1.25×10^{10} cm$^{-2}<\rho\leqslant10\times10^{10}$ cm^{-2}. That is, over this range of densities, the results depend significantly on the basis size. The reason for this lack of convergence will be discussed in Sec. V. As a result, we are not able to directly reproduce the saturation of the redshift and subsequent small blueshift found in the experimental results at moderate densities. However, as we shall show in the next section, our nonperturbative formalism at very high densities shows that there must be a redshift saturation followed by a blueshift due to plasma oscillations, in qualitative agreement with experiment.

To further examine the density dependence of the emitted THz radiation, we plot in Fig. 7 the normalized THz power spectra for different densities for experiment and theory. In

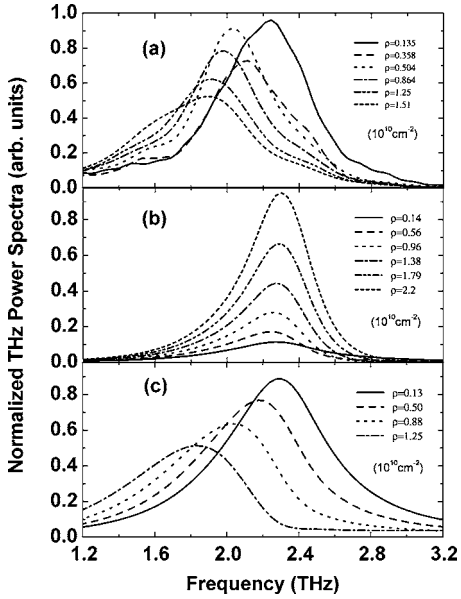

FIG. 7. The normalized THz power spectra (power spectra divided by the square of the density) for different exciton areal densities from (a) experiment, (b) fourth-order calculation, and (c) nonperturbative calculations.

all of these, we are plotting the power spectrum of the normalized emitted THz field—i.e., the emitted THz power spectrum divided by the square of the density. In Fig. 7(a), we plot the experimental spectra for different densities. We see that the total normalized THz energy generally decreases as the density increases. The decrease is monotonic, except for the density of $\rho=0.358\times10^{10}$ cm^{-2}, which seems to have an anomalously low power. We are not certain of the reason for this, but we have sometimes found similar results in our nonperturbative simulations under different conditions.

In Figs. 7(b) and 7(c), we plot the normalized power spectra calculated using the fourth-order and nonperturbative methods. The nonperturbative results are in good agreement with the experimental results, with the normalized THz energy decreasing roughly linearly with density. In the fourth-order results, however, the normalized spectral peaks height are *increasing* with exciton density, which is in complete contradiction to the experimental results.

In Fig. 8 we plot the integration of the normalized THz spectral density (Fig. 7) as a function of density for experiment and theory. This gives the THz energy emitted divided by the square of the density. The experimental and theoretical energies are set equal at low density to facilitate comparison. We have also included the second-order results, for which the normalized energy does not change with density. This is as expected, because for a set of identical coherent radiators, the radiated power should increase with the square of the density. This is essentially the phenomena of Dicke superradiance. As can be seen, the nonperturbative results agree very well with the experimental ones, whereas the fourth-order results predict the opposite trend. Note that the fourth-order results for the emitted energy are even worse than the second-order ones. This is just like the situation when one attempts to expand an expression in a power series

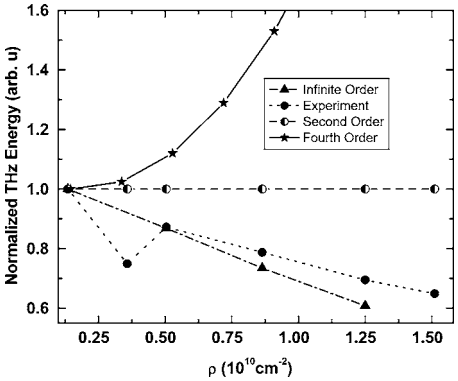

FIG. 8. The normalized THz energy emitted (integrated THz power divided by the square of the density) for the experimental and theoretical results as a function of the areal density.

when it is outside its radius of convergence: the higher-order expansion will often give even worse result than that of low-order expansions. This is yet another indication that we are well beyond the perturbative regime for this structure.

In summary, we find that the nonperturbative formalism gives results that are in good agreement with experiment, while the fourth-order calculations not only underestimate the frequency redshift in the low-density limit, but also greatly overestimate the emitted THz radiation power. The perturbation method is valid only when the excited exciton densities is well below its corresponding critical value. Otherwise, higher-order perturbation methods will give even worse results than lower-order perturbation ones. We find that for our structure, the critical value for exciton density is roughly $\rho=0.2\times10^{10}$ cm^{-2}. In next section, we will show that in addition to accounting for the redshift in the low-density limit, the nonperturbative formalism also predicts blueshift in the high-density limit where collective excitations (coherent plasma oscillations) occur due to dynamic exciton-exciton interactions.

V. PLASMA OSCILLATIONS

In this section, we examine the THz emission at the very high densities ($\rho\geqslant10\times10^{10}$ cm^{-2}), where our calculations are again convergent. As we shall show, our nonperturbative formalism predicts the appearance of coherent PO's at these high exciton densities.[45–47]

As has been pointed out by previous authors,[45] when the density is high enough, such that the plasma frequency in the superlattice is comparable to the BO frequency, we expect the BO's to evolve into PO's. This is accounted for in our theory via the ac portion of the self-induced internal field $\mathbf{E}_{\text{intra}}$ in Eq. (13), which provides a restoring force when the electrons and holes are pulled apart. At low densities, PO's are not evident because the restoring force is too small to have a significant effect on the BO's. However, at high densities the restoring force causes the electrons to return to the holes before they have a chance to perform even a single BO. In other words, once this restoring force dominates over the net effect of the applied dc field and the periodic superlattice

potential, the nonperturbative formalism predicts PO's.

Now we turn to the details of the transition process from BO's to coherent PO's. As mentioned in previous sections, the nonperturbative formalism presented in this work does not converge for intermediate exciton densities. We find, however, that in both the low- and high-exciton-density limits our formalism gives results that do not depend significantly on the basis size used (i.e., the results are converged) once we employ a basis that includes two-well states with along-axis electron-hole separation up to $8d$ (and hence allows for the calculation of excitonic WSL states with $|n| \leq 8$). The reason for the lack of convergence at intermediate densities can be understood by considering exciton dynamics in ac and dc fields. In the nonperturbative formalism, BO's are driven by the self-induced internal field $\mathbf{E}_{\text{intra}}$, which has both dc and ac components [see Eq. (13)]. In these combined fields, it has been shown that the exciton population is driven to the superlattice boundaries corresponding to higher single-particle WSL ladder indices $|n|$ due to the Shapiro effect.[10,17] This driving of the population is essentially due to the absorption and/or emission of THz photons, which cause transitions among the WSL states. Thus, there is a rapid driving apart of the electrons and holes, moving them to the boundaries of superlattice. Our formalism assumes that the superlattice is infinite, with the maximum electron-hole separation in the z direction determined by the size of the calculation basis employed (maximum electron-hole separation in two-well exciton states employed). If a basis of infinite size is used, the carriers are driven until dephasing and population decay finally stops the process. However, at intermediate densities this requires a prohibitively large basis set, which in fact represents a superlattice that has more periods than the one being experimentally investigated (50). Therefore, we are unable to achieve converged results at these intermediate densities.

At very high densities, the problem of population driving is greatly mitigated and essentially disappears when the induced internal dc field E_{dc} becomes very large and approaches its natural limit: $E_{dc} \rightarrow -F_o$. As can be seen from Fig. 2, this limit is reached when $\rho \gtrsim 10 \times 10^{10}$ cm^{-2} (see Fig. 2). In this case, the self-induced internal dc field cancels the external dc field completely[40] and thus there is essentially no longer a WSL in the BSSL. Thus excitons are not driven to the superlattice boundaries anymore and the nonperturbative formalism leads to converged results in the high-density limit. We also note that because the net dc field is very small at high densities, the PO's exhibited are not competing with Wannier-Stark localization and so the dynamics are much like one would expect in an unbiased superlattice. The initial perturbation to the electron-hole gas is provided by the initial conditions given by the optical pulse, which generates electrons and holes that are initially separated and subsequently undergo PO's.

In Fig. 9, we plot the THz oscillation frequency as a function of exciton density for a wide range of densities. The experimental results and the simulations using both nonperturbative and fourth-order calculations are all presented in the same figure for clear comparison. In the low-density limit, the intraband dynamics are dominated by BO's and we can see a good agreement between experimental results

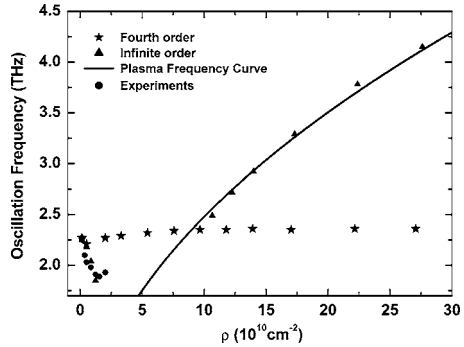

FIG. 9. Peak THz frequency as a function of the exciton areal density for the experimental results, fourth-order calculations, nonperturbative (infinite order) calculations, and the expression from standard plasma theory [Eq. (23)].

and the nonperturbative calculations (also shown in Fig. 6). For intermediate densities, there is no convergence for the nonperturbative calculations. However, when $\rho > 10 \times 10^{10}$ cm^{-2}, the nonperturbative results converge, and it is these results that we present. As discussed above, these results essentially describe the coherent PO's arising from the many-body interactions among excitons. As we have neglected PSF effects, it is expected that these high-density results will only be qualitatively correct. However, as we discuss in the Conclusion, it is reasonable to expect that such effects will only have a large effect on the initial conditions (e.g., through absorption saturation), but not on the basic effect of PO's.

The usual expression for the plasma frequency is

$$\omega_{pl} = \sqrt{\frac{e^2 n_0}{\epsilon m_{pl}^*}}, \tag{23}$$

where $n_0 = \rho d$ is the volume density and m_{pl}^* is the reduced effective plasma mass for the electron-hole pairs. Taking the plasma mass to be a fitting parameter, we find that we obtain an excellent fit to the nonperturbative results using Eq. (23) with a plasma mass of $m_{pl}^* = 0.125\ m_o$, where m_o is the free-electron mass (see Fig. 9). Now, the expected plasma effective mass can be estimated to be the reduced electron-hole miniband effective mass in the BSSL at band bottom. In the nearest-neighbor tight-binding approximation this mass is given by

$$\frac{1}{m_{pl}^*} = \frac{\Delta d^2}{2\hbar^2}, \tag{24}$$

where $\Delta \simeq 43$ meV is the combined electron-hole miniband width. Thus for our BSSL, we obtain

$$m_{pl}^* \simeq 0.050 m_o. \tag{25}$$

We note that this miniband effective mass is about half that used in Eq. (23) to fit the nonperturbative results in Fig. 9. This discrepancy is largely due to the fact that the effective mass in Eq. (24) is obtained by setting $k = 0$. However, in our nonperturbative calculations, the electrons and holes are op-

tically excited into states that contain components with k far from $k=0$.[10] Thus it is not appropriate to simply use the effective mass at miniband minimum to determine the plasma effective mass, and we expect the plasma mass to be considerably larger than that given by Eq. (25). In fact we find (not shown) that the best-fit plasma effective mass depends considerably on the initial conditions. This is consistent with the above argument, since the k-space distribution is different for different initial conditions.[10] However, we note that the PO's do not change much.

We also present the fourth-order calculations in Fig. 9. We note that the fourth-order calculation converges over the full density range. However, as seen in Fig. 9, the fourth-order simulation initially gives only a tiny redshift and then approaches a constant frequency as exciton density increases. Thus, it fails to account correctly for the redshift at low densities and the PO's at high densities.

The generation of PO's in our nonperturbative calculations demonstrates that our formalism inherently includes dynamic screening as discussed above. Recent theoretical and experimental results suggest that the dynamic response time of the carriers is given approximately by the inverse of the PO frequency.[42–44] Thus, as is discussed in the previous section, if we extrapolate the PO frequency given by Eq. (23) down to the lower densities, we expect that dynamic screening will start to significantly affect the THz emission for densities larger than or on the order of $\rho=5\times10^{9}$ cm^{-2}.

From the results presented in Fig. 9, we can now understand the origin of the saturation of the frequency redshift seen in the experimental results (Figs. 5, 6, and 9): at densities of about $\rho=2\times10^{10}$ cm^{-2}, the BO's are starting to transform into plasma oscillations. This transformation is not seen directly in our calculations because our nonperturbative calculations do not converge for densities in the range 1.25×10^{10} cm$^{-2}<\rho\leqslant10\times10^{10}$ cm^{-2}. However, from the results of our converged low- and high-density calculations, we can infer that there must be a frequency region where the oscillation frequency saturates and eventually blueshifts. This, therefore, provides a qualitative explanation of the experimental results at the higher densities and points to the possibility of experimentally observing *pure* PO's at higher densities still.

Although we have presented experimental evidence of the transition from BO's to PO's, we were unable to experimentally access the high carrier densities ($\rho\gtrsim10^{11}$ cm^{-2}) needed to observe *pure* PO's in our BSSL. There were two factors limiting the maximum densities that we could achieve. In general photogenerated carriers travel to the contacts and partially screen the applied dc field by collecting on the superlattice barrier layers. We generally can compensate for this screening voltage by simply increasing the applied external voltage. However, for high densities, the required external voltages are so large that the back-biased Schottky contact at the surface of our samples breaks down. This was one major factor limiting the maximum density at which we could operate. The second factor was excitation-induced dephasing (EID). At high densities, the linewidths of the interband transitions increase strongly due to EID. This line broadening made it very difficult to keep the internal field constant by monitoring the weak-pulse absorption spectrum, as the transitions were barely detectable at very high densities.

If the technical difficulties in experimentally achieving the high densities required to see pure PO's could be overcome, it still is not entirely clear if pure PO's would be observed. There are two factors that might affect the theoretical predictions at high densities: the neglect of PSF effects[18,27] and EID. PSF effects are proportional to ρ/ρ_0, where ρ_0 is the inverse of the single $1s$ exciton area. In this work, at the density of $\rho=10\times10^{10}$ cm^{-2} at which pure PO's begin to appear, $\rho/\rho_0\simeq0.5$. This indicates that the PSF effects will likely be important in the case of pure PO's. However, as PO's are clearly seen in much higher-density systems, it is expected that the main effect of PSF will be to alter the excitation conditions (initial condition); it should not affect the existence of PO's themselves. Thus, we expect that PO's will survive in the presence of PSF effects, as is indirectly evidenced by recent theory and experiments.[42–44] The effect of EID on intraband dephasing times is another factor that could affect the observation of pure PO's. Although EID seems to have a large effect on the decay of the *interband* polarization when the densities reach $\rho=2\times10^{10}$ cm^{-2} (see above), its effect on the *intraband* polarization dephasing seems to be considerably less: the intraband dephasing time did not change much for densities up to at least $\rho=2\times10^{10}$ cm^{-2} (see Fig. 5). Furthermore, recent theoretical and experimental results[48,49] indicate that the EID rate should only increase as $\rho^{1/3}$ at high densities. Thus, we are hopeful that *pure* PO's will eventually be seen at high densities in BSSL's.

VI. CONCLUSIONS

We have presented theoretical and experimental results for the emitted THz radiation from biased semiconductor superlattices excited via an ultrashort optical pulse. We have demonstrated, by comparing the perturbative and nonperturbative optical responses, that a formalism that is nonperturbative in the optical field is necessary to explain the experimental results. Perturbation theory is only valid when the exciting optical intensity is very low ($\rho<0.2\times10^{10}$ cm^{-2} for our system). The source of the nonlinearity leading to the frequency shifts is the strong exciton-exciton interaction in the BSSL, which arises from the broken symmetry induced by the external dc field. We found both experimentally and by using the nonperturbative formalism that the THz frequency is strongly dependent on exciton density: as the density increases, the frequency first redshifts; then, the redshift saturates and finally undergoes a blueshift. We attribute the saturation and final blueshift to the evolution of Bloch oscillations into plasma oscillations. Two features are crucial to theoretically account for the experimental phenomena in a tractable way. First, by using an exciton basis, second-order Coulomb correlations were approximately included under the framework of a first-order cluster expansion. Second, the dynamics were treated nonperturbatively in the optical field so as to self-consistently include the self-generated local fields that can considerably renormalize the original eigenstates and thus dynamics in intense optical excitations.

ACKNOWLEDGMENTS

The authors thank Karl Leo for fruitful discussions and support for the experimental portion of this work. This work was supported in part by the Natural Sciences and Engineering Research Council of Canada and by Deutsche Forschungsgemeinschaft (Grants No. Le 747/11 and the Leibniz Preis).

[1] J. Shah, *Ultrafast Spectroscopy of Semiconductors and Semiconductor Nanostructures*, 2nd enlarged ed. (Springer, Berlin, 1999).
[2] D. S. Chemla and J. Shah, Nature (London) **411**, 549 (2001).
[3] H. Haug and S. W. Koch, *Quantum Theory of the Optical and Electronic Properties of Semiconductors*, 3rd ed. (World Scientific, Singapore, 1994).
[4] H. Haug and A.-P. Jauho, *Quantum Kinetics in Transport and Optics of Semiconductors* (Springer, Berlin, 1996).
[5] H. Haug, in *Ultrafast Physical Progresses in Semiconductors*, edited by K. T. Tsen, Semiconductors and Semimetals, Vol. 67 (Academic, San Diego, 2001), p. 205.
[6] V. M. Axt, G. Bartels, and A. Stahl, Phys. Rev. Lett. **76**, 2543 (1996).
[7] G. Bartels, G. C. Cho, T. Dekorsy, H. Kurz, A. Stahl, and K. Köhler, Phys. Rev. B **55**, 16404 (1997).
[8] F. Rossi and T. Kuhn, Rev. Mod. Phys. **74**, 895 (2002).
[9] J. Hader, T. Meier, S. W. Koch, F. Rossi, and N. Linder, Phys. Rev. B **55**, 13799 (1997).
[10] F. Löser, M. M. Dignam, Yu. A. Kosevich, K. Köhler, and K. Leo, Phys. Rev. Lett. **85**, 4763 (2000).
[11] V. M. Axt and S. Mukamel, Rev. Mod. Phys. **70**, 145 (1998).
[12] Th. Östreich, K. Schönhammer, and L. J. Sham, Phys. Rev. B **58**, 12920 (1998).
[13] C. Sieh, T. Meier, F. Jahnke, A. Knorr, S. W. Koch, P. Brick, M. Hübner, C. Ell, J. Prineas, G. Khitrova, and H. M. Gibbs, Phys. Rev. Lett. **82**, 3112 (1999); C. Sieh, T. Meier, A. Knorr, F. Jahnke, P. Thomas, and S. W. Koch, Eur. Phys. J. B **11**, 407 (1999).
[14] T. Meier, S. W. Koch, P. Brick, C. Ell, G. Khitrova, and H. M. Gibbs, Phys. Rev. B **62**, 4218 (2000).
[15] V. G. Lyssenko, G. Valusis, F. Loser, T. Hascha, K. Leo, M. M. Dignam, and K. Kohler, Phys. Rev. Lett. **79**, 301 (1997).
[16] L. Yang, B. Rosam, J. M. Lachaine, K. Leo, M. M. Dignam, Phys. Rev. B **69**, 165310 (2004).
[17] J. M. Lachaine, Margaret Hawton, J. E. Sipe, and M. M. Dignam, Phys. Rev. B **62**, R4829 (2000).
[18] M. M. Dignam, M. Hawton, Phys. Rev. B **67**, 035329 (2003).
[19] V. M. Axt and T. Kuhn, Rep. Prog. Phys. **67**, 433 (2004).
[20] T. Meier, G. von Plessen, P. Thomas, and S. W. Koch, Phys. Rev. Lett. **73**, 902 (1994).
[21] P. H. Bolivar, F. Wolter, A. Muller, H. G. Roskos, H. Kurz, and K. Köhler, Phys. Rev. Lett. **78**, 2232 (1997).
[22] L. Bányai, Q. T. Vu, B. Mieck, and H. Haug, Phys. Rev. Lett. **81**, 882 (1998).
[23] P. Gartner, L. Bányai, and H. Haug, Phys. Rev. B **62**, 7116 (2000).
[24] N.-Hang Kwong and M. Bonitz, Phys. Rev. Lett. **84**, 1768 (2000).
[25] U. Hohenester and W. Pötz, Phys. Rev. B **56**, 13177 (1997).
[26] T. Wolterink, V. M. Axt, and T. Kuhn, Phys. Rev. B **67**, 115311 (2003).
[27] M. Hawton and M. M. Dignam, Phys. Rev. Lett. **91**, 267402 (2003).
[28] S. B. de-Leon and B. Laikhtman, Phys. Rev. B **63**, 125306 (2001).
[29] M. Combescot and O. Betbeder-Matibet, Europhys. Lett. **58**, 87 (2002).
[30] Undergoing projects and will be published in the future.
[31] L. Esaki and R. Tsu, IBM J. Res. Dev. **14**, 61 (1970).
[32] E. E. Mendez, F. Agulló-Rueda, and J. M. Hong, Phys. Rev. Lett. **60**, 2426 (1988).
[33] C. Waschke, P. Leisching, P. H. Bolivar, R. Schwedler, F. Brüggemann, H. G. Roscos, K. Leo, H. Kurz, and K. Köhler, Solid-State Electron. **37**, 1321 (1994).
[34] M. M. Dignam and J. E. Sipe, Phys. Rev. B **41**, 2865 (1990).
[35] B. Rosam, L. Yang, K. Leo, and M. M. Dignam, Appl. Phys. Lett. **85**, 4612 (2004).
[36] V. Chernyak, W. M. Zhang, and S. Mukamel, J. Chem. Phys. **109**, 9587 (1998).
[37] Q. Wu and X.-C Zhang, Appl. Phys. Lett. **68**, 1604 (1996).
[38] A. Leitenstorfer, S. Hunsche, J. Shah, M. C. Nuss, and W. H. Knox, Appl. Phys. Lett. **74**, 1516 (1999).
[39] Q. Wu and X.-C Zhang, Appl. Phys. Lett. **71**, 1285 (1997).
[40] D. Turchinovich, P. U. Jepsen, B. S. Monozon, M. Koch, S. Lahmann, U. Rossow, and A. Hangleiter, Phys. Rev. B **68**, 241307(R) (2003).
[41] G. C. Cho, A. Ziebell, T. Dekorsy, H. J. Bakker, B. Opitz, A. Kohl, and H. Kurz, J. Appl. Phys. **82**, 4400 (1997).
[42] L. Bányai, Q. T. Vu, B. Mieck, and H. Haug, Phys. Rev. Lett. **81**, 882 (1998).
[43] K. El Sayed, S. Schuster, H. Haug, F. Herzel, and K. Henneberger, Phys. Rev. B **49**, 7337 (1994).
[44] R. Huber, F. Tauser, A. Brodschelm, M. Bichler, G. Abstreiter, and A. Leitenstorfer, Nature (London) **414**, 286 (2001).
[45] A. W. Ghosh, L. Jönsson, and J. W. Wilkins, Phys. Rev. Lett. **85**, 1084 (2000).
[46] F. Löser, Y. A. Kosevich, K. Köhler, and K. Leo, Phys. Rev. B **61**, R13373 (2000).
[47] K. Leo, P. Haring Bolivar, F. Brüggemann, R. Schwedler, and K. Köhler, Solid State Commun. **84**, 943 (1992).
[48] W. A. Hügel, M. F. Heinrich, M. Wegener, Q. T. Vu, L. Bányai, and H. Haug, Phys. Rev. Lett. **83**, 3313 (1999).
[49] B. Mieck, H. Haug, W. A. Hügel, M. F. Heinrich, and M. Wegener, Phys. Rev. B **62**, 2686 (2000).